

## Vibration analysis of prestressed concrete bridge subjected to moving vehicles

M. Huang<sup>1</sup>, J.K. Liu<sup>2\*</sup>, S.S. Law<sup>3</sup> and Z.R. Lu<sup>2</sup>

<sup>1</sup>*Research Center of Intelligent Transportation System, Sun Yat-sen University, Guangzhou, Guangdong Province, 510006, P.R.China*

<sup>2</sup>*Department of Applied Mechanics and Engineering, Sun Yat-sen University, Guangzhou, Guangdong Province, 510006, P.R. China*

<sup>3</sup>*Civil and Structural Engineering Department, Hong Kong Polytechnic University, Hungghom, Kowloon, Hong Kong, P.R. China*

*(Received August 16, 2011, Revised November 2, 2011, Accepted November 3, 2011)*

**Abstract.** The vibration response of the bridges under the moving vehicular load is of importance for engineers to estimate the serviceability of existing bridges and to design new bridges. This paper deals with the three dimensional vibration analysis of prestressed concrete bridges under moving vehicles. The prestressed bridges are modeled by four-node isoparametric flat shell elements with the transverse shearing deformation taken into account. The usual five degrees-of-freedom (DOFs) per node of the element are appended with a drilling DOF to accommodate the transformation of the local stiffness and mass matrices to the global coordinates. The vehicle is modeled as a single or two-DOF system. A single-span prestressed Tee beam and two-span prestressed box-girder bridge are studied as the two numerical examples. The effects of prestress forces on the natural frequencies and dynamic responses of the bridges are investigated.

**Keywords:** prestressed concrete bridge; flat shell element; drilling degree-of-freedom; box-girder; vehicle-bridge interaction.

---

### 1. Introduction

The bridge vibration caused by the passing of vehicles or trains has received considerable attention for many decades (Akin and Mofid 1989, Hwang and Nowak 1991, Yang and Lin 1995, Yang and Yau 1997, Law and Zhu 2005, Stavridis 2008, Stull and Earls 2009, Yau 2009, Chang *et al.* 2010, Wang *et al.* 2010, Li and Zhu 2010, Yang *et al.* 2010). The researches can be classified into the following categories: the suspension system of the vehicle, road surface roughness, bridge span length, the effect of vehicle braking, axle spacing of the vehicle, gross vehicle weight, vehicle moving speed, unit mass of the bridge and bridge damping. Many approaches have been developed to study the influence of various factors on the dynamic behavior of the bridge.

The bridge structure has been modeled with the finite element method using the beam element (Wang and Huang 1992, Law and Zhu 2005), grillage method (Wang *et al.* 1993, Huang *et al.* 1993,

---

\* Corresponding author, Professor, E-mail: [liujike@mail.sysu.edu.cn](mailto:liujike@mail.sysu.edu.cn)

Tan *et al.* 1997), eight-node quadrilateral Kirchhoff plate/shell element and three-node Euler-Bernoulli beam (Fafard *et al.* 1998, Henchi *et al.* 1998), and as an assemblage of beam and plate elements (Chompooming and Yener 1995). Recently, Lee and Yhim (2005) studied the dynamic response of continuous box girder bridges subjected to moving loads using the folded flat shell element.

In analyzing the bridge-vehicle interaction system, two sets of equations of motion must be written each for the bridge and for the vehicle. It is the interaction forces existing at the contact points that make the two subsystems coupled. As the contact points move from time to time, the system matrices are time-dependent and must be updated at each time step in calculating the dynamic response. The equations of motion of the bridge and the vehicle are solved separately by an iterative procedure (Yang and Fonder 1996). In the study by Henchi *et al.* (1998), the coupled equations were directly by the central difference method. To solve this problem, a vehicle-bridge interaction element was developed by Yang and Lin (1995) and Yang and Yau (1997).

The prestressed concrete box-girder bridges have been widely used as an economic and aesthetic solutions for the crossings over deep valleys or other traffic lines, for which relatively long spans have been used. However, the effect of the prestressing forces on the dynamic behavior of the structures has not been fully investigated. Amongst the literature on the dynamic analysis of bridges under moving vehicles, the bridge has been idealized mostly as a beam structure (Pisani 1996, Law and Lu 2005). However, for box-girder bridges, such a simplified beam model cannot fully describe the behavior at the cross-section of the box girder. Lee and Yhim (2005) have carried out an investigation on the dynamic behavior of long span box girder bridges under moving vehicles, along with experiments on a prestressed box girder bridge. In this study, the moving vehicle is simply replaced by the moving load, while no attention was paid to the effect of prestressing forces on the dynamic behavior of the bridge.

In this paper, the effects of prestressing forces on the dynamic behaviour of the bridges are investigated by the 3-dimensional finite element analysis. The bridge is modeled by four-node isoparametric flat shell elements with account taken of the transverse shearing deformation. The usual five degrees-of-freedom (DOFs) per node of the element are appended with a drilling DOF to accommodate the transformation of the local stiffness and mass matrices to the global coordinates. The bonded prestressing tendon is modeled by 2-node truss elements (with 3 DOFs per node) embedded in the flat shell element. The moving vehicle is modeled as a single or two-DOF system. A single-span Tee beam and two-span prestressed box-girder bridges are studied as the two examples, for which the results obtained are compared with those generated by the commercial software ANSYS. The effects of prestressing force on the natural frequencies and dynamic response of the bridge are studied. The effect of road roughness on the dynamic responses of the bridge and vehicle is also taken into account.

## 2. Finite element formulation

### 2.1 The displacement field

The flat shell element with five DOFs per node can be obtained by superimposing the planar stress element on the plate bending element (Bathe 1996). For the planar stress element, we have

$$\begin{Bmatrix} u \\ v \end{Bmatrix} = \sum_{i=1}^n N_i^{(m)} a_i^{(m)}, \quad a_i^{(m)} = \begin{Bmatrix} u_i \\ v_i \end{Bmatrix} \quad (i = 1, 2, \dots, N) \quad (1)$$

where  $N$  is the number of nodes of the element,  $N_i^{(m)}$  is the isoparametric shape function of the plane stress element. For plate bending, we have

$$\begin{Bmatrix} w \\ \theta_x \\ \theta_y \end{Bmatrix} = \sum_{i=1}^N \begin{bmatrix} N_i^{(m)} & 0 & 0 \\ 0 & N_i^{(\theta_x)} & 0 \\ 0 & 0 & N_i^{(\theta_y)} \end{bmatrix} a_i^{(b)}, \quad a_i^{(b)} = \begin{Bmatrix} w_i \\ (\theta_x)_i \\ (\theta_y)_i \end{Bmatrix} \quad (i = 1, 2, \dots, N) \quad (2)$$

Combining Eqs. (1) and (2)

$$U = \begin{Bmatrix} u \\ v \\ w \\ \theta_x \\ \theta_y \end{Bmatrix} = \Theta a \quad (3)$$

where

$$a = \begin{Bmatrix} a_1 \\ a_2 \\ a_3 \\ \vdots \\ a_N \end{Bmatrix}, \quad a_i = \begin{Bmatrix} u_i \\ v_i \\ w_i \\ (\theta_x)_i \\ (\theta_y)_i \end{Bmatrix}, \quad \Theta = [\Theta_1, \Theta_2, \dots, \Theta_N]$$

$$\Theta_i = \begin{bmatrix} N_{ui}^{(m)} & & & & \\ & N_{vi}^{(m)} & & & \\ & & N_i^{(w)} & & \\ & & & N_i^{(\theta_x)} & \\ & & & & N_i^{(\theta_y)} \end{bmatrix} \quad (3a)$$

### 2.2 The strains

The strains of the flat shell include the in-plane membrane strains  $\varepsilon^p$ , the curvature owing to bending  $\varepsilon^b$ , and the transverse shearing strains  $\varepsilon^s$ . The in-plane membrane strains are

$$\boldsymbol{\varepsilon}^p = \begin{Bmatrix} \varepsilon_x \\ \varepsilon_y \\ \gamma_{xy} \end{Bmatrix} = \begin{Bmatrix} \frac{\partial u}{\partial x} \\ \frac{\partial v}{\partial y} \\ \frac{\partial v}{\partial x} + \frac{\partial u}{\partial y} \end{Bmatrix} \quad (4)$$

the strain due to bending can be written as

$$\boldsymbol{\varepsilon}_b = -z \begin{Bmatrix} \kappa_x \\ \kappa_y \\ \kappa_{xy} \end{Bmatrix} = -z \begin{Bmatrix} \frac{\partial \theta_x}{\partial x} \\ \frac{\partial \theta_y}{\partial y} \\ \frac{\partial \theta_x}{\partial y} + \frac{\partial \theta_y}{\partial x} \end{Bmatrix} \quad (5)$$

and the transverse shearing strains are

$$\boldsymbol{\varepsilon}^s = \begin{Bmatrix} \gamma_{xz} \\ \gamma_{yz} \end{Bmatrix} = \begin{Bmatrix} \frac{\partial w}{\partial x} - \theta_x \\ \frac{\partial w}{\partial y} - \theta_y \end{Bmatrix} \quad (6)$$

The variations of all the above strains can be written as

$$\delta \boldsymbol{\varepsilon}^p = \begin{Bmatrix} \delta \left( \frac{\partial u}{\partial x} \right) \\ \delta \left( \frac{\partial v}{\partial y} \right) \\ \delta \left( \frac{\partial u}{\partial y} \right) + \delta \left( \frac{\partial v}{\partial x} \right) \end{Bmatrix} \quad (7)$$

$$\delta \boldsymbol{\varepsilon}^b = -z \begin{Bmatrix} \delta \left( \frac{\partial \theta_x}{\partial x} \right) \\ \delta \left( \frac{\partial \theta_y}{\partial y} \right) \\ \delta \left( \frac{\partial \theta_y}{\partial x} \right) + \delta \left( \frac{\partial \theta_x}{\partial y} \right) \end{Bmatrix} \quad (8)$$

$$\delta \boldsymbol{\varepsilon}^s = \begin{Bmatrix} -\delta \theta_x + \delta \left( \frac{\partial w}{\partial x} \right) \\ -\delta \theta_y + \delta \left( \frac{\partial w}{\partial y} \right) \end{Bmatrix} \quad (9)$$

The expressions for the strain-displacement relations can be deduced from Eqs. (7)-(9) as

$$\delta \boldsymbol{\varepsilon}^p = \sum_{i=1}^N \begin{bmatrix} N_{i,x}^{(m)} & & \\ & N_{i,y}^{(m)} & \\ N_{i,y}^{(m)} & N_{i,x}^{(m)} & \end{bmatrix} \begin{Bmatrix} \delta u_i \\ \delta v_i \end{Bmatrix} = \sum_{i=1}^N B_i \delta a_i^{(m)} \quad (10)$$

$$\delta \boldsymbol{\varepsilon}^s = \sum_{i=1}^N \begin{bmatrix} N_{i,x}^w & -N_i^\theta & 0 \\ N_{i,y}^w & 0 & -N_i^\theta \end{bmatrix} \begin{Bmatrix} \delta w_i \\ \delta(\theta_x)_i \\ \delta(\theta_y)_i \end{Bmatrix} = \sum_{i=1}^N B_i^s \delta a_i^{(b)} \quad (11)$$

$$\delta \boldsymbol{\varepsilon}^b = \sum_{i=1}^N \begin{bmatrix} 0 & N_{i,x}^\theta & 0 \\ 0 & 0 & N_{i,y}^\theta \\ 0 & N_{i,y}^\theta & N_{i,x}^\theta \end{bmatrix} \begin{Bmatrix} \delta w_i \\ \delta(\theta_x)_i \\ \delta(\theta_y)_i \end{Bmatrix} = \sum_{i=1}^N B_i^b \delta a_i^{(b)} \quad (12)$$

### 2.3 The elemental mass and stiffness matrices

The consistent mass matrix for the element used to model the concrete box-girder bridge can be expressed as

$$m^e = \int_A \boldsymbol{\Theta}^T \rho_m \boldsymbol{\Theta} dA \quad (13)$$

where

$$\rho_m = \begin{bmatrix} \rho t & 0 & 0 & 0 & 0 & 0 \\ 0 & \rho t & 0 & 0 & 0 & 0 \\ 0 & 0 & \rho t & 0 & 0 & 0 \\ 0 & 0 & 0 & \frac{\rho t^3}{12} & 0 & 0 \\ 0 & 0 & 0 & 0 & \frac{\rho t^3}{12} & 0 \\ 0 & 0 & 0 & 0 & 0 & 0 \end{bmatrix}$$

It is known that the global stiffness matrix is singular or ill-conditioned because of the null diagonal terms due to the drilling DOF in the transformed elemental stiffness matrix. To solve this problem, a rotational stiffness coefficient will be artificially inserted in the diagonal corresponding to the drilling DOF in this paper, as was done by Lee and Yhim (2005).

The elemental stiffness matrix of the concrete bridge is expressed as

$$K_e = \int_A (B_i^p)^T D^p B_j^p dA + \int_A (B_i^s)^T D^s B_j^s dA + \int_A (B_i^b)^T D^b B_j^b dA + \int_A G_i^T \begin{bmatrix} T_{x0}^p & 0 \\ 0 & T_{y0}^p \end{bmatrix} G_j dA \quad (14)$$

where,  $G_i = \begin{bmatrix} N_{i,x}^u & N_{i,x}^v & N_{i,x}^w & 0 & 0 & 0 \\ N_{i,y}^u & N_{i,y}^v & N_{i,y}^w & 0 & 0 & 0 \end{bmatrix}$ ,  $T_{x0}^p$  and  $T_{y0}^p$  are the two components of the prestressing force along the  $x$  and  $y$  axis, respectively.

#### 2.4 Including of the prestressing tendon

##### 2.4.1 The elemental stiffness matrix of the tendon

Fig. 1 shows a segment of the prestressing tendon embedded into a flat shell element. Noting that only the axial deformation of the tendon needs to be considered. In this regard, the 3-D truss element is used to model the prestressing tendon. The elemental stiffness of the tendon in terms of the local coordinates can be expressed as

$$[k_e] = \frac{E_s A_s}{l} \begin{bmatrix} 1 & 0 & 0 & -1 & 0 & 0 \\ 0 & 0 & 0 & 0 & 0 & 0 \\ 0 & 0 & 0 & 0 & 0 & 0 \\ -1 & 0 & 0 & 1 & 0 & 0 \\ 0 & 0 & 0 & 0 & 0 & 0 \\ 0 & 0 & 0 & 0 & 0 & 0 \end{bmatrix} \quad (15)$$

The transformation matrix between the local and global coordinates systems is given as

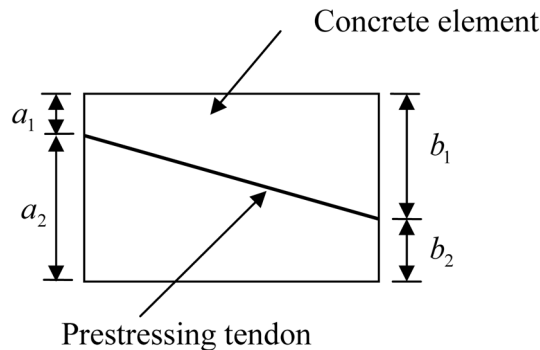


Fig. 1 Prestressing tendon embedded into a concrete element

$$T = \begin{bmatrix} L & 0 \\ 0 & L \end{bmatrix} \tag{16}$$

where  $L = \begin{bmatrix} \xi_1 & \xi_2 & \xi_3 \\ \eta_1 & \eta_2 & \eta_3 \\ \varsigma_1 & \varsigma_2 & \varsigma_3 \end{bmatrix}$ ,  $\{\xi_1 \eta_1 \varsigma_1\}$  denotes the direction cosines of the  $\bar{x}$ -axis with respect to the

$xyz$ -coordinate system. Similarly,  $\{\xi_2 \eta_2 \varsigma_2\}$  and  $\{\xi_3 \eta_3 \varsigma_3\}$  are the direction cosines of the  $\bar{y}$ -axis and  $\bar{z}$ -axis with respect to the  $xyz$ -coordinate system, respectively.

By performing the transformation between the local and global coordinates, the elemental stiffness matrix can be expressed in the global coordinates as

$$[\bar{k}_e] = [T]^T [k_e] [T] \tag{17}$$

Since  $[\bar{k}_e]$  is a matrix with a dimension of  $6 \times 6$ , the dimension of the elemental stiffness matrix of the shell element is of  $24 \times 24$ . A transformation matrix is needed to expand the matrix  $[\bar{k}_e]$  into the matrix of  $24 \times 24$ . The transformation matrix is expressed as

$$TR = \begin{bmatrix} \frac{a_2}{l_1} & 0 & 0 & 0 & 0 & 0 & 0 & 0 & 0 & 0 & 0 & 0 & 0 & 0 & 0 & 0 & \frac{a_1}{l_1} & 0 & 0 & 0 & 0 & 0 \\ 0 & \frac{a_2}{l_1} & 0 & 0 & 0 & 0 & 0 & 0 & 0 & 0 & 0 & 0 & 0 & 0 & 0 & 0 & \frac{a_1}{l_1} & 0 & 0 & 0 & 0 & 0 \\ 0 & 0 & \frac{a_2}{l_1} & 0 & 0 & 0 & 0 & 0 & 0 & 0 & 0 & 0 & 0 & 0 & 0 & 0 & 0 & \frac{a_1}{l_1} & 0 & 0 & 0 & 0 \\ 0 & 0 & 0 & 0 & 0 & 0 & \frac{b_2}{l_2} & 0 & 0 & 0 & 0 & \frac{b_1}{l_2} & 0 & 0 & 0 & 0 & 0 & 0 & 0 & 0 & 0 & 0 \\ 0 & 0 & 0 & 0 & 0 & 0 & \frac{b_2}{l_2} & 0 & 0 & 0 & 0 & \frac{b_1}{l_2} & 0 & 0 & 0 & 0 & 0 & 0 & 0 & 0 & 0 & 0 \\ 0 & 0 & 0 & 0 & 0 & 0 & 0 & \frac{b_2}{l_2} & 0 & 0 & 0 & 0 & \frac{b_1}{l_2} & 0 & 0 & 0 & 0 & 0 & 0 & 0 & 0 & 0 \end{bmatrix} \tag{18}$$

$$K_{es} = [TR]^T [\bar{k}_e] [TR] \tag{19}$$

#### 2.4.2 The elemental mass matrix of the tendon

The consistent mass matrix for the space truss element is

$$[\bar{m}_e] = \frac{\rho A I}{6} \begin{bmatrix} 2\xi_1^2 & 2\xi_1\xi_2 & 2\xi_1\xi_3 & \xi_1^2 & \xi_1\xi_2 & \xi_1\xi_3 \\ 2\xi_1\xi_2 & 2\xi_2^2 & 2\xi_2\xi_3 & \xi_1\xi_2 & \xi_2^2 & \xi_2\xi_3 \\ 2\xi_1\xi_3 & 2\xi_2\xi_3 & 2\xi_3^2 & \xi_1\xi_3 & \xi_2\xi_3 & \xi_3^2 \\ \xi_1^2 & \xi_1\xi_2 & \xi_1\xi_3 & 2\xi_1^2 & 2\xi_1\xi_2 & 2\xi_1\xi_3 \\ \xi_1\xi_2 & \xi_2^2 & \xi_1\xi_3 & 2\xi_1\xi_2 & 2\xi_2^2 & 2\xi_2\xi_3 \\ \xi_1\xi_3 & \xi_1\xi_3 & \xi_3^2 & 2\xi_1\xi_3 & 2\xi_2\xi_3 & 2\xi_3^2 \end{bmatrix} \quad (20)$$

Similarly, the elemental mass matrix can be expanded into a matrix of  $24 \times 24$  as follows

$$M_{es} = [TR]^T [\bar{m}_e] [TR] \quad (21)$$

## 2.5 Linear free vibration analysis of the prestressed concrete bridge

Elemental stiffness matrix of the prestressed concrete bridge for linear free vibration analysis is expressed as

$$K_e = \int_A (B_i^p)^T D^p B_j^p dA + \int_A (B_i^s)^T D^s B_j^s dA + \int_A (B_i^b)^T D^b B_j^b dA + \int_A G_i^T \begin{bmatrix} T_{x0}^p & 0 \\ 0 & T_{y0}^p \end{bmatrix} G_j dA + K_{es} \quad (22)$$

The first term on the right hand side of Eq. (22) is the stiffness matrix for the plate in planar stress, the second term is the one associated with the transverse shear, the third term is related to the effect of bending, the fourth term is the geometric stiffness due to the prestressing force, and the fifth term is the stiffness due to the prestressing tendon.

The elemental mass matrix for the linear free vibration analysis of the bridge is expressed as

$$M_e = m_e + M_{es} \quad (23)$$

By assembling all the elemental matrices in the global coordinates, the eigen equation for the free vibration analysis of the bridge is

$$K_b U = \lambda M_b U \quad (24)$$

where  $K_b$  is the global stiffness matrix, and  $M_b$  is the global mass matrix of the bridge. The eigen values  $\lambda$  and eigen vectors  $U$  of the bridge can be obtained by solving Eq. (24).

## 2.6 Linear forced vibration analysis of the bridge-vehicle systems

### 2.6.1 Equation of motion for the bridge

The equation of motion for the linear forced vibration equation of the bridge under moving vehicles is expressed as

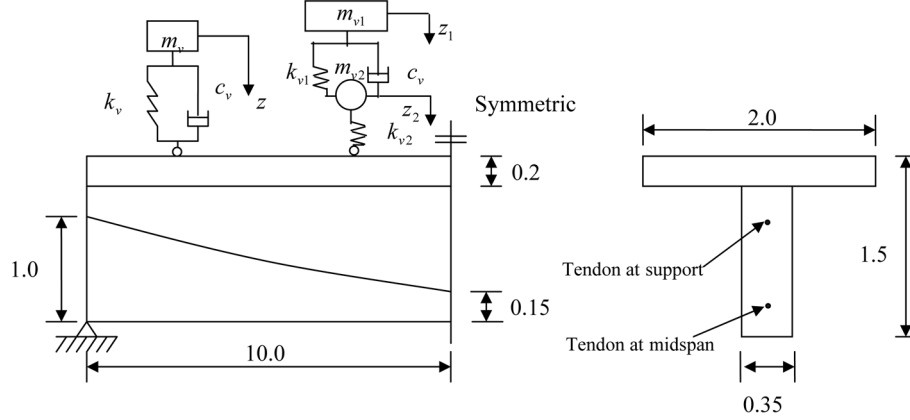


Fig. 2 Vehicle models and geometry of the simply supported Tee beam (dimensions in meter)

$$M_b \ddot{d} + C_b \dot{d} + K_b d = H_c P_{\text{int}} \quad (25)$$

where  $C_b$  is the damping matrix determined as  $C = \alpha_1 M_b + \alpha_2 K_b$ , with two constants  $\alpha_1$  and  $\alpha_2$ , based on the Rayleigh damping model;  $\ddot{d}$ ,  $\dot{d}$  and  $d$  are the acceleration velocity and displacement responses of the structure, respectively;  $P_{\text{int}}$  is the interaction force between the bridge and the vehicle; and  $H_c$  is a matrix with zero entries except for the DOFs corresponding to the nodal displacements of the shell elements on which the load is acting.

### 2.6.2 Equation of motion for the vehicle: 3-parameter vehicle model

The three-parameter model shown in Fig. 2 for the vehicle is a single DOF system, which comprises a mass connected with a damper and a spring. The equation of motion of the vehicle is

$$m_v \ddot{z} + c_v (\dot{z} - \dot{\hat{w}}(x, y, t)) + k_v (z - \hat{w}(x, y, t) - r(x, y)) = 0 \quad (26)$$

where  $\ddot{z}$ ,  $\dot{z}$  and  $z$  are the vertical acceleration, velocity and displacement responses of the vehicle, respectively, and  $m_v$ ,  $c_v$  and  $k_v$  are the mass, damping and stiffness of the vehicle, respectively. The variable  $\hat{w}(x, y, t)$  represents the vertical deflection of the contact point of the vehicle with the bridge, as denoted by the transverse and longitudinal coordinates  $x$  and  $y$ .  $r(x, y)$  is the road surface roughness at the location of the tyre (ISO 1995). It should be pointed out that in Eq. (26), the additional velocity and acceleration due to road surface roughness may be taken into account to determine the movement of the vehicle wheel as discussed by Chang *et al.* (2011). In the present study, as the speed of the moving vehicle is not high, the effect of high-frequency vibrations caused by the modeling of the wheels as points, compared with disks, is believed to negligible.

The vehicle-bridge interaction force  $P_{\text{int}}$  is expressed as

$$P_{\text{int}} = m_v g + c_v (\dot{z} - \dot{\hat{w}}(x, y, t)) + k_v (z - \hat{w}(x, y, t) - r(x, y)) = m_v g - m_v \ddot{z} \quad (27)$$

where  $g$  is the acceleration of gravity. The vehicle is assumed to be in perfect contact with the bridge deck all the time, i.e. no jumps occur between the wheels and the bridge. Combining Eqs. (25) and (26), the equation of motion of the vehicle-bridge system is written as

$$\begin{bmatrix} M_b & H_c m_v \\ 0 & m_v \end{bmatrix} \begin{Bmatrix} \ddot{d} \\ \ddot{z} \end{Bmatrix} + \begin{bmatrix} C_b & 0 \\ -H_c^T c_v & c_v \end{bmatrix} \begin{Bmatrix} \dot{d} \\ \dot{z} \end{Bmatrix} + \begin{bmatrix} K_b & 0 \\ -H_c^T k_v & k_v \end{bmatrix} \begin{Bmatrix} d \\ z \end{Bmatrix} = \begin{Bmatrix} H_c m_v g \\ k_v r(x, y) \end{Bmatrix} \quad (28)$$

The dynamic responses of the bridge and vehicle can be solved in a step-by-step manner using the state space method (Juang 1994).

### 2.6.3 Equation of motion for the vehicle: 5-parameter vehicle model

The five-parameter model shown in Fig. 2 for the vehicle is a two-DOF system, which comprises five components: an upper mass  $m_{v1}$  of the suspension, a lower mass  $m_{v2}$  of the bogie and axle connected to the suspension damper  $c_v$  and a suspension spring  $k_{v1}$ , together with another spring  $k_{v2}$  used to represent the stiffness of the tyre. The equations of motion of the masses  $m_{v1}$  and  $m_{v2}$  of the vehicle can be written as

$$m_{v1} \dot{z}_1 + c_v (\dot{z}_1 - \dot{z}_2) + k_{v1} (z_1 - z_2) = 0 \quad (29a)$$

$$m_{v2} \ddot{z}_2 + c_v (\dot{z}_2 - \dot{z}_1) + k_{v1} (z_2 - z_1) + k_{v2} (z_2 - (w(x, y, t) + r(x, y))) = 0 \quad (29b)$$

where  $\ddot{z}_1$ ,  $\dot{z}_1$  and  $z_1$  are the vertical acceleration, velocity and displacement responses of the suspension mass of vehicle, respectively, and  $\ddot{z}_2$ ,  $\dot{z}_2$  and  $z_2$  are the vertical acceleration, velocity and displacement responses of the bogie and axle. The interaction force  $P_{\text{int}}$  between the bridge and the vehicle can be expressed as

$$P_{\text{int}} = (m_{v1} + m_{v2})g + k_{v2} (z_2 - (w(x, y, t) + r(x, y))) = (m_{v1} + m_{v2})g - m_{v1} \ddot{z}_1 - m_{v2} \ddot{z}_2 \quad (30)$$

Similarly, one can combine Eqs. (25) and (29) in compact form and establish the coupled equation of motion for the vehicle-bridge system as

$$\begin{bmatrix} M_b & H_c m_{v1} & H_c m_{v2} \\ 0 & m_{v1} & 0 \\ 0 & 0 & m_{v2} \end{bmatrix} \begin{Bmatrix} \ddot{d} \\ \ddot{z}_1 \\ \ddot{z}_2 \end{Bmatrix} + \begin{bmatrix} C_b & 0 & 0 \\ 0 & c_v & -c_v \\ 0 & -c_v & c_v \end{bmatrix} \begin{Bmatrix} \dot{d} \\ \dot{z}_1 \\ \dot{z}_2 \end{Bmatrix} + \begin{bmatrix} K_b & 0 & 0 \\ 0 & k_{v1} & -k_{v1} \\ -H_c^T k_{v2} & -k_{v1} & k_{v1} + k_{v2} \end{bmatrix} \begin{Bmatrix} d \\ z_1 \\ z_2 \end{Bmatrix} = \begin{Bmatrix} H_c (m_{v1} + m_{v2})g \\ 0 \\ k_{v2} r(x, y) \end{Bmatrix} \quad (31)$$

## 3. Numerical simulations

### 3.1 A prestressed Tee beam

The prestressed tee beam studied by Figueiras and Povoas (1994) is used as a numerical example in this paper. The beam is a 20 meter span T beam, simply supported and prestressed with a

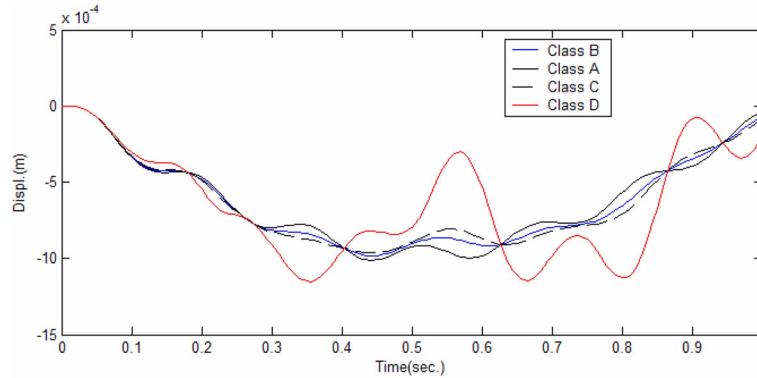


Fig. 3 Effect of road roughness on the displacement responses of the beam

parabolic tendon. The geometry of the beam is shown in Fig. 3. The mechanical properties of the concrete are: Young's modulus  $E_c = 3.4 \times 10^{10}$  Pa, mass density  $\rho_c = 2800$  kg/m<sup>3</sup>, Poisson ratio  $\nu = 0.18$ . The mechanical properties of the prestressing tendon are: Young's modulus  $E_p = 210$  GPa, mass density  $\rho_p = 7800$  kg/m<sup>3</sup>. The magnitude of the prestressing force is 3 MN and the prestressing tendon is assumed to be perfectly bonded and no prestress loss is taken into account.

In the present finite element modeling of the beam, the flange is discretized into two 4-node isoparametric flat shell elements in the transverse direction and 20 elements in the longitudinal direction. The web is discretized into 20 elements in the longitudinal direction.

### 3.1.1 Free vibration of the beam

#### The drilling DOF

First of all, free vibration is conducted for the beam. As mentioned before, the system stiffness is singular because of the null diagonal terms due to the drilling DOF in the transformed elemental stiffness matrix. Based on the work by Lee and Yhim (2005), the optimal stiffness  $\gamma_k$  for the drilling DOF is taken as  $10 \times 10^8$  in this paper. Table 1 gives a comparison on the first eight natural frequencies computed from the modal analysis of the unprestressed beam using the commercial software package ANSYS. Here, the Shell63 element is used in the finite element simulation of the beam. As for the finite element mesh, the flange is discretized into 18 elements in the longitudinal direction and 2 elements in the transverse direction. The web is discretized into 18 elements in the longitudinal direction and 1 element in the transverse direction. The finite element mesh for the beam used by ANSYS is the same as that of the present finite element model. From Table 1, one can see that the first natural frequencies computed herein match well with those by ANSYS, which indicates the validity of the present finite element formulation.

#### The effect of prestressing force on natural frequencies

When the beam is prestressed with a magnitude of 3 MN prestressing force, the first eight natural frequencies computed of the prestressed beam are listed in Table 1 and compared with those obtained by ANSYS. In order to model the parabolic prestressing tendon, the mesh for the web of the prestressed beam is different from the model for the unprestressed beam used by ANSYS mentioned in the preceding section. To allow consideration of the prestressing tendon in this case

Table 1 Natural frequencies of tee beam obtained by the present approach and by ANSYS

Mode	Unprestressed		Prestressed (parabolic tendon)		Prestressed (straight tendon)	
	FEM	ANSYS	FEM	ANSYS	FEM	ANSYS
1	6.372	6.065	6.3	6.113	6.257	6.008
2	7.626	7.433	7.441	7.145	7.486	7.316
3	8.25	8.477	8.268	8.425	8.215	8.359
4	21.735	20.881	21.545	19.928	21.548	20.745
5	21.991	21.809	21.923	21.415	21.901	21.735
6	24.279	24.526	24.243	24.519	24.243	24.363
7	35.176	33.772	35.075	30.297	35.087	33.798
8	37.029	37.556	36.847	36.422	36.846	37.405
9	47.162	46.513	47.075	46.695	47.074	46.225

using ANSYS, the web of the beam is discretized into 11 layers along the vertical direction and 18 elements in the longitudinal direction. The tendon is represented by the Link8 element in the ANSYS model. The nodes of the tendon are located at the intersection points of the parabolic curve and the layers of the web. In order to further compare the natural frequencies from the present finite element model and those from ANSYS, a straight prestressing tendon is adopted. The tendon is assumed to pass through the common nodes of the flange and the web and this time the mesh of ANSYS and the present finite element model is the same. Table 1 gives a comparison on the natural frequencies computed by the present model and those by ANSYS, which indicates that the two results are consistent.

### 3.1.2 Forced vibration of bridge under moving vehicle: 3-parameter vehicle model

The properties adopted of the 3-parameter vehicle model are:  $m_v = 4.0 \times 10^3$  kg,  $c_v = 1.0 \times 10^3$  Ns/m. The traveling speed of the vehicle is 20 m/s and the time step is 0.005 s. Class A to D road surface roughness is considered herein. Fig. 3 gives a comparison on the displacement response of the vehicle and that at the middle point of the flange for different road roughness conditions. From this figure one can see that the road roughness condition has significant effect on the responses of both the bridge and the vehicle. It also seems that the road roughness has more significant effect on the vehicle than on the bridge. Fig. 4 shows the displacement response at the middle point of the flange of the beam with and without prestressing force. This figure indicates that the prestressing force has large effect on the bridge response.

### 3.2 Prestressed box girder

A two-span prestressed continuous box-girder bridge is studied in this numerical example, as shown in Fig. 5. The dimensions of the bridge are shown in Fig. 5. The physical properties adopted of the bridge are: Young's modulus  $E = 3.4 \times 10^{10}$  Pa, and mass density  $\rho = 2.5 \times 10^3$  kg/m<sup>3</sup>. The bridge is assumed to be jacked at both end, with a prestressing force of  $T = 4MN$  exerted through the jack. The prestressing tendon has a parabolic shape. The prestress loss is taken into account. Table 2 shows the prestressing force in each of the 20 elements used to model the web.

In the present finite element of the bridge, the upper plate of bridge is discretized into six 4-node isoparametric flat shell elements in the transverse direction and 20 elements in the longitudinal direction. The bottom plate of the bridge is discretized into 2 elements in the transverse direction

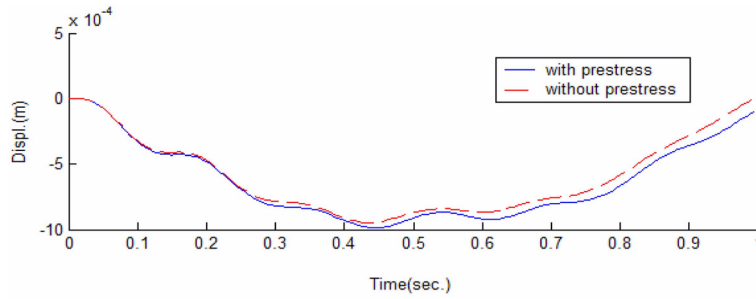


Fig. 4 Effect of prestressing force on the displacement response of the beam (mid span of the beam)

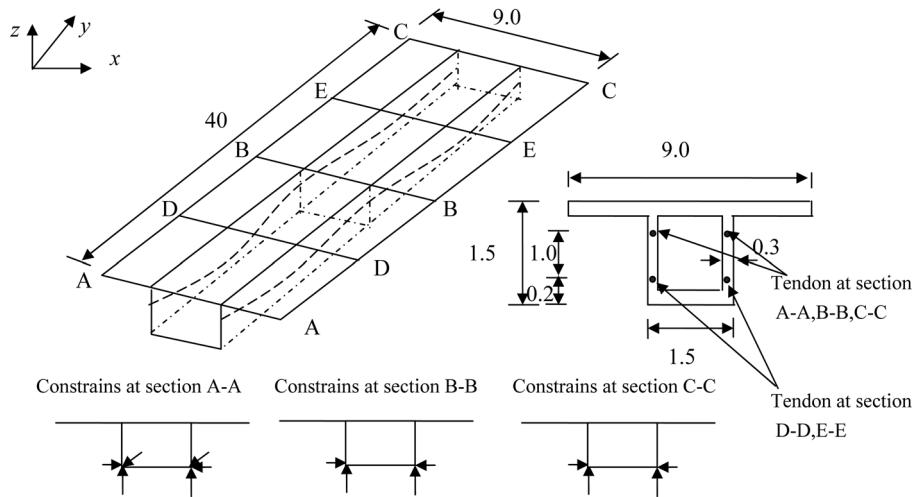


Fig. 5 Two-span prestressed box girder bridge (Dimensions in meter)

Table 2 Value of prestressing force in each element

Element No.	1	2	3	4	5	6	7	8	9	10
Prestress (MN)	4.0	3.88	3.76	3.64	3.52	3.40	3.28	3.12	2.96	2.8
Element No.	11	12	13	14	15	16	17	18	19	20
Prestress (MN)	2.8	2.96	3.12	3.28	3.40	3.52	3.64	3.76	3.88	4.0

and 20 elements in the longitudinal direction. The ribs are discretized into 20 elements in the longitudinal direction.

### 3.2.1 Free vibration of the bridge

Again, free vibration analysis is conducted for the box girder bridge first. The optimal stiffness  $\gamma_k$  chosen for the drilling DOF is the same as that used in the first numerical example. Table 3 gives a comparison on the first 10 natural frequencies of the bridge with different magnitudes of prestressing force exerted at the jack and for the case with no prestressing force. From this table,

Table 3 Natural frequencies of box girder with different prestressing forces

Mode	Unprestressed	4MN	8MN	10MN
1	7.442	7.411	7.380	7.365
2	9.469	9.459	9.449	9.445
3	9.948	9.927	9.905	9.894
4	10.899	10.898	10.896	10.896
5	15.753	15.750	15.748	15.747
6	15.886	15.882	15.877	15.875
7	16.445	16.441	16.438	16.436
8	16.787	16.783	16.779	16.777
9	16.983	16.982	16.981	16.981
10	18.372	18.369	18.365	18.364

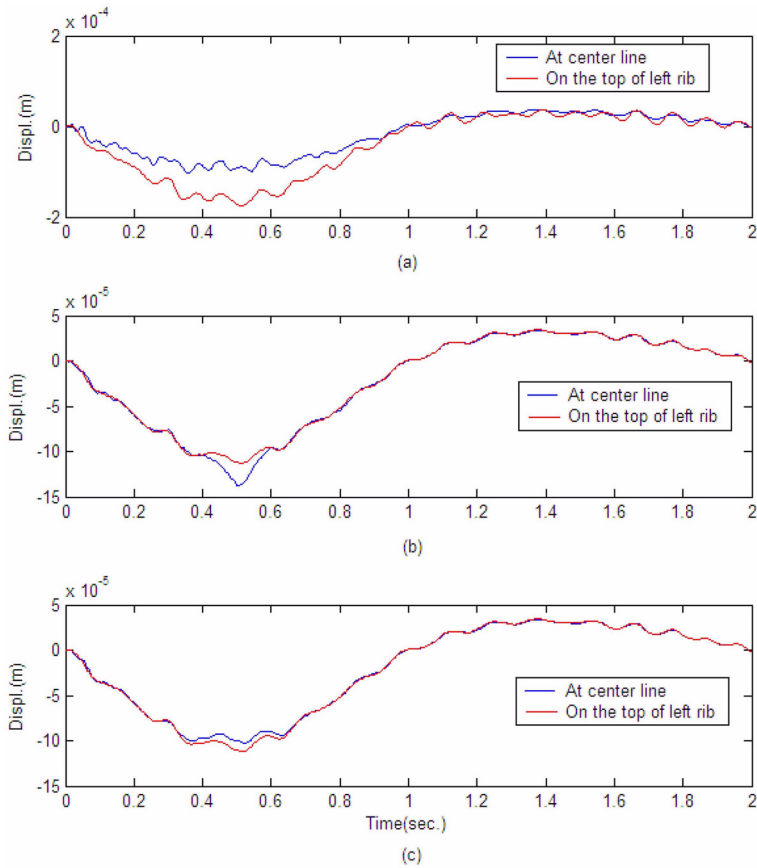


Fig. 6 Effect of vehicle location on the displacement response at different points: (a) L/4 of the left edge line, (b) L/4 of the center line of top plate and (c) L/4 of the center line of the bottom plate

one can see that the effect of the prestressing force on the natural frequencies of the bridge becomes significant as the magnitude of the prestressing force increases.

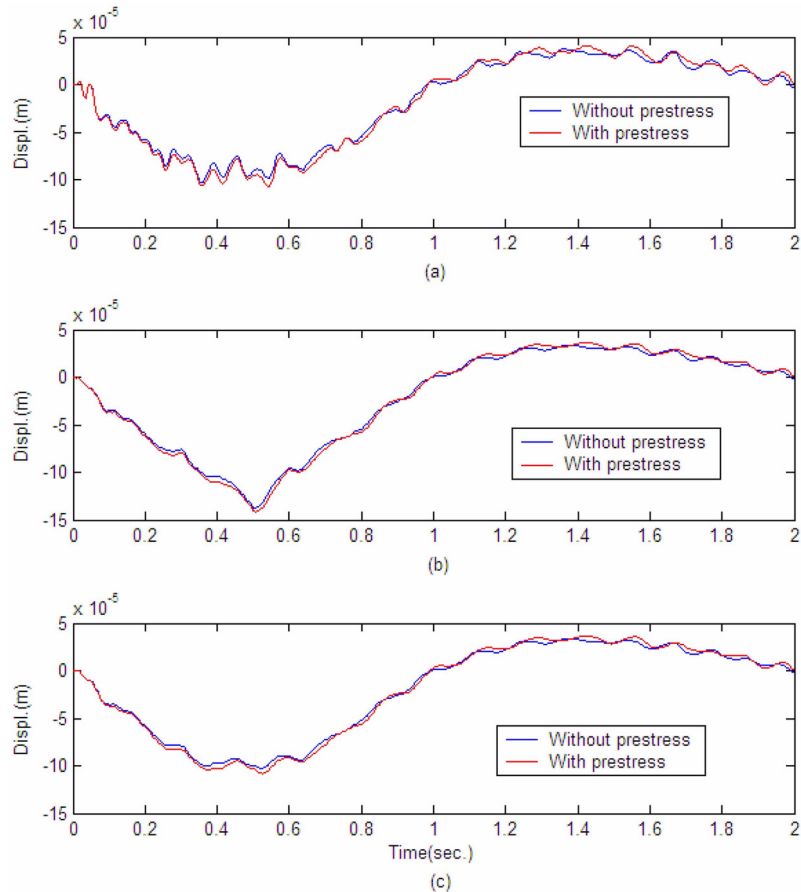


Fig. 7 Effect of prestressing force on the displacement at different locations of the section: (a) L/4 of the left edge line, (b) L/4 of the center line of top plate and (c) L/4 of the center line of the bottom plate

### 3.2.2 Forced vibration of bridge under moving vehicle: 5-parameter vehicle model

#### Effect of the location of the vehicle on the response

The properties adopted of the 5-parameter vehicle model are:  $m_{v1} = 3.6 \times 10^3$  kg,  $m_{v2} = 0.25 \times 10^3$  kg,  $c_v = 1.0 \times 10^3$  Ns/m,  $k_{v1} = 6.0 \times 10^5$  N/m,  $k_{v2} = 8.5 \times 10^5$  N/m. The traveling speed of the vehicle is 20 m/s and the time step is 0.005 s. Class B road surface is adopted. Two cases are studied: (a) the vehicle moves on top of the left vertical rib, (b) the vehicle moves along the centre line of the bridge deck.

Fig. 6 gives a comparison on the displacement responses at three different points of the section at 10 m (L/4) from the left support of the bridge. From this figure, one can see that when the vehicle moves along different paths, the dynamic responses of different nodes at the same cross section are different. When the vehicle moves along the centre line of the bridge deck, the response at the point of L/4 of the center line of top plate is much greater than the response at the point of L/4 of the left edge line. In other words, a larger response will be induced by the vehicle moving along the centre line of the bridge for the points of concern.

### Effect of prestressing force on the responses at different locations in a section of the bridge

It is known that the dynamic responses at different locations in a section are different for a box girder. In this section, the effect of the prestressing force on the responses at different locations of a section of the box-girder bridge is studied. Fig. 7 shows the displacement response at the different points of the bridge with and without prestressing force, when the magnitude of the prestressing force exerted at the jack is 20 MN. It seems from this figure that when the magnitude of the prestressing force is relatively large, its effect on the responses of bridge will increase significantly.

## 4. Conclusions

The dynamic analysis of prestressed concrete bridges subjected to moving vehicles is carried out by using a three-dimensional finite element analysis with the bridge modeled by the flat shell elements. The vehicle is modeled as a single or two degree-of-freedom system. The dynamic responses are computed for the vehicle-bridge interaction system by a step-by-step integration approach. The effect of prestressing force on the dynamic response of the vehicle-bridge coupled system is investigated. The numerical simulations indicate that with the increase of the prestressing force, the natural frequencies of the bridge decrease, and the dynamic responses of the bridge increase. Thus, the prestressing force cannot be neglected when its magnitude is relatively high. This paper also reveals that for the vehicle moving along the centre line of the bridge deck, the response at the center line of top plate at the location of  $L/4$  from the left support of the beam is greater than the responses at the other points of the same cross-section.

## Acknowledgements

This work is supported in part by the NSFC (11172333, 10972241), GDSF (07003680, 9151027501000014), the Guangdong Province Science and Technology Program (2010A030200008, 2011A030200012), Doctoral Program Foundation of Ministry of Education of China (20090171110042), and the Fundamental Research Funds for the Central Universities (09lgpy08). Such financial aids are gratefully acknowledged.

## References

- Akin, J.E. and Mofid, M. (1989), "Numerical solution for response of beams with moving mass", *J. Struct. Eng.* - *ASCE*, **115**(1), 120-131.
- Bathe, K.J. (1996), *Finite element procedures in engineering analysis*, Prentice Hall, New Jersey.
- Chang, K.C., Wu, F.B. and Yang, Y.B. (2010), "Effect of road surface roughness on indirect approach for measuring bridge frequencies from a passing vehicle", *Interact. Multiscale Mech.*, **3**(4), 299-308.
- Chang, K.C., Wu, F.B. and Yang, Y.B. (2011), "Disk model for wheels moving over highway bridges with rough surfaces", *J. Sound Vib.*, **330**, 4930-4944.
- Chompooming, K. and Yener, M. (1995), "The influence of roadway surface irregularities and vehicle deceleration on bridge dynamics using the method of lines", *J. Sound Vib.*, **183**(4), 567-589.
- Fafard, M., Savard, M. and Bennur, M. (1998), "Dynamic analysis of existing continuous bridge", *J. Bridge Eng.* - *ASCE*, **3**(1), 28-37.

- Figueiras, J.A. and Povoas, R.H.C.F. (1994), "Modeling of prestress in non-linear analysis of concrete structures", *Comput. Struct.*, **53**(1), 173-187.
- Henchi, K., Fafard, M., Talbot, M. and Dhatt, G. (1998), "An efficient algorithm for dynamic analysis of bridge under moving vehicles using a coupled modal and physical components approach", *J. Sound Vib.*, **212**(4), 663-683.
- Huang, D.Z., Wang, T.L. and Shahawy, M. (1993), "Impact studies of multi-concrete bridges", *J. Struct. Eng. - ASCE*, **119**(21), 2387-2402.
- Hwang, E.S. and Nowak, A.S. (1991), "Simulation of dynamic load for bridges", *J. Struct. Eng. - ASCE*, **117**(5), 1413-1434.
- ISO 8608: 1995(E), Mechanical vibration - road surface profiles - reporting of measured data.
- Juang, J.N. (1994), *Applied system identification*, New Jersey.
- Law, S.S. and Zhu, X.Q. (2005), "Bridge dynamic responses due to road surface roughness and braking of vehicle", *J. Sound Vib.*, **282**, 805-830.
- Law, S.S. and Lu, Z.R. (2005), "Time domain responses of a prestressed beam and prestress identification", *J. Sound Vib.*, **288**, 1011-1025.
- Lee, S.Y. and Yhim, S.S. (2005), "Dynamic behavior of long-span box girder bridges subjected to moving loads: numerical analysis and experimental verification", *Int. J. Soilds Struct.*, **42**, 5021-5035.
- Li, X.Z. and Zhu, Y. (2010), "Stochastic space vibration analysis of a train-bridge coupling system", *Interact. Multiscale Mech.*, **3**(4), 333-342.
- Pisani, M.A. (1996), "A numerical model for externally prestressed beams", *Struct. Eng. Mech.*, **4**(2), 177-190.
- Stavridis, Leonidas T. (2008), "A simplified analysis of the behavior of suspension bridges under live load", *Struct. Eng. Mech.*, **30**(5), 559-576.
- Stull, C.J. and Earls, C.J. (2009), "A rapid assessment methodology for bridges damaged by truck strikes", *Steel Compos. Struct.*, **9**(3), 223-237.
- Yang, F. and Fonder, G.A. (1996), "An iterative solution method for dynamic response of bridge-vehicle systems", *Earthq. Eng. Struct. Dyn.*, **25**, 195-215.
- Yang, J.R., Li, J.Z. and Chen, Y.H. (2010), "Vibration analysis of CFST tied-arch bridge due to moving vehicles", *Interact. Multiscale Mech.*, **3**(4), 389-403.
- Yang, Y.B. and Lin, B.H. (1995), "Vehicle-bridge interaction analysis by dynamic condensation method", *J. Struct. Eng. - ASCE*, **121**(11), 1636-1643.
- Yang, Y.B. and Yau, J.D. (1997), "Vehicle-bridge interaction element for dynamic analysis", *J. Struct. Eng. - ASCE*, **123**(11), 1512-1518.
- Yau, J.D. (2009), "Vehicle/bridge interactions of a rail suspension bridge considering support movements", *Interact. Multiscale Mech.*, **2**(3), 263-276.
- Wang, T.L. and Huang, D.Z. (1992), "Cable-stayed bridge vibration due to road roughness", *J. Struct. Eng. - ASCE*, **118**(5), 1354-1374.
- Wang, T.L., Huang, D.Z. and Shahawy, M. (1993), "Dynamic response of multi-girder bridges", *J. Struct. Eng. - ASCE*, **118**(8), 2222-2238.
- Wang, S.Q., Xia, H., Guo, W.W. and Zhang, N. (2010), "Nonlinear dynamic response analysis of a long-span suspension bridge under running train and turbulent wind", *Interact. Multiscale Mech.*, **3**(4), 309-320.